Third International Conference on CFD in the Minerals and Process Industries
CSIRO, Melbourne, Australia
10-12 December 2003

CFD SIMULATION OF BUBBLE FLOWS UNDER VARYING PATTERNS IN HORIZONTAL PIPES FOR PYRITE OXIDATION

Congli Cheng, Moses O. Tadé, Vishnu Pareek

Department of Chemical Engineering, Curtin University of Technology
GPO Box U 1987, Perth WA 6845, Australia

ABSTRACT

Regarding the pyrite oxidation process as a gas pseudo-liquid flow system, a two-phase multi-component CFD (Computational Fluid Dynamics) model has been developed. Depending on the operating conditions, several flow patterns may appear in horizontal pipes for pyrite oxidation. In this paper, flow characteristics of the dispersed bubble flow and the buoyant bubble flow were studied by the CFD model respectively. The simulation profiles for the local void fraction and velocities of the buoyant bubble flow are consistent with the experimental investigations conducted by other authors under a similar flow system. Distinct differences of dynamics exist between the two flow patterns. In the dispersed bubble flow, the gas mixture forms a boundary layer near the wall, while in the buoyant bubble flow the gas mixture tends to move from the pipe bottom to the pipe top.

Keywords: Pyrite oxidation; CFD; flow patterns; Horizontal pipes;

NOMENCLATURE

A	pre-exponential factor
C	molar concentration or drag coefficient
d	bubble diameter
D	kinematic diffusivity
E	water evaporation rate coefficient
Ea	activation energy
F	interface drag force
h	enthalpy
H	molar heat
k	mass transfer rate or chemical reaction rate
k_H	Henry constant of water
M	mass sources
P	pressure
q	heat flux
Q	interphase heat transfer
R	universal gas constant or reaction rate
S	heat source
T	temperature
u	velocity
W	molar weight
Y	mass fraction of component
$ø$	volume fraction
ρ	density
σ	surface tension
τ	viscous stress

INTRODUCTION

Currently fine pyrite particles mixed with dilute sulphuric acid are oxidized by oxygen gas in autoclaves. Having the advantages such as larger interfacial areas between reactants, less costs and fewer agitating apparatus, horizontal pipe reactors have been proposed as alternatives for autoclaves. The fluids involved in pyrite oxidation system include three phases, respectively, gas mixture, liquid mixture and solid particles. Any multi-phase flow, as long as it contains the gas phase, appears as a certain flow pattern determined by the operating conditions. With respect to the concept of flow patterns, solutions to three questions have been being hunting researchers for many years (Li and Kwauk, 1994; Govier and Aziz, 1972; Weller, 1985). They are respectively: (1) how to define a flow pattern? (2) what is the dynamics for certain flow patterns? (3) how to judge the transition between two neighbouring flow patterns? A great deal of reports relating to these three questions have been published. Unfortunately there is no conclusive agreement among these reports because of the complex nature of the system caused by the distinctive differences of properties between the gas phase and the other phases. This paper attempts to provide solutions to the first two questions. Theoretical and experimental work still needs to be done to address some of the fundamental issues.

PHYSICAL PROCESSES AND CHEMICAL REACTION IN PYRITE OXIDATION

As an approximation, liquid mixture and solid particles are normally integrated as a so-called pseudo-liquid (Felice, 2000; Hua et al., 2000; Govier and Aziz, 1972). Therefore the gas-liquid-solid three-phase flow of pyrite oxidation is simplified to a gas-liquid two-phase flow. The physical processes and chemical reaction occurring in a micro-element are illustrated in Figure 1.

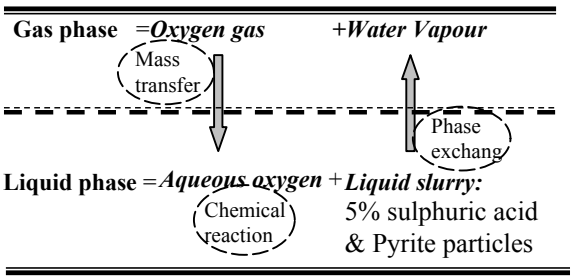

Figure 1: Multi-phase multi-component representation of the pyrite oxidation process

Mass transfer of oxygen from the gas phase to the liquid phase

In term of the theory of mass transfer, oxygen transfer from the gas phase to the liquid phase is driven by the concentration difference of oxygen between the gas-liquid interface and the bulk liquid phase. In the unit of $kg/(m^3 \cdot s)$, a universal oxygen transfer rate can be written as:

$$M_{O_2,tran} = k_{O_2}\left(C_{O_2,il} - C_{O_2,bl}\right)W_{O_2}\phi_l \quad (1)$$

where W_{O_2} is oxygen molar mass, $C_{O_2,il}$ and $C_{O_2,bl}$ are oxygen molar concentration at gas-liquid interface and in bulk liquid respectively, ϕ_l is the volume fraction of the liquid phase, k_{O_2} is oxygen volumetric mass transfer coefficient. Rubisov and Papangelakis (1995) gave the expressions for k_{O_2} and $C_{O_2,il}$ as follows respectively:

$$k_{O_2} = 0.5667 \exp\left(\frac{500}{463} - \frac{500}{T_l}\right) \quad (2)$$

where T_l is the liquid phase temperature.

$$C_{O_2,il} = \frac{P_{O_2}}{k_H} \quad (3)$$

P_{O_2} is the partial pressure of oxygen in gas mixture, and Henry constant k_H is given as:

$$k_H = \frac{10^9}{\rho_{H_2O}} \exp\left(\begin{array}{l} -15.98 + \dfrac{1.58\times10^4}{T_l} \\ -\dfrac{4.333\times10^6}{T_l^2} + \dfrac{3.502\times10^8}{T_l^3} \end{array}\right) \quad (4)$$

where ρ_{H_2O} is the water density.

As oxygen gas enters the liquid phase, some energy is simultaneously brought into the liquid phase by the physical process of oxygen mass transfer. In the unit of $J/m^3 \cdot s$, the heat flux by oxygen transfer is given as:

$$S_{O_2,tran} = M_{O_2,tran}\Delta H_{O_2,tran}/W_{O_2} \quad (5)$$

$\Delta H_{O_2,tran}$ is the enthalpy change produced by a molar oxygen transferred from the gas phase to the liquid phase, with a value of –11.75 kJ/mol.

Water evaporation from the liquid phase to the gas phase

Zhang et al. (2001), Carey (1992) and Eames et al. (1997) presented a correlation for water evaporation in bubble flow systems with non-flat concave interface, which is different from the correlation for a flat surface. In the unit of $kg/(m^3 \cdot s)$, water evaporation rate of a concave interface surface can be written as:

$$M_{H_2O,evap} = \frac{2E}{2-E}\sqrt{\frac{W_{H_2O}}{2\pi RT_g}} \left[1 - \exp\left(-\frac{4\sigma W_{H_2O}}{d_b \rho_{H_2O} RT_l}\right)\right] P_{sat} \frac{6\phi_g\phi_l}{d_b} \quad (6)$$

where E is the evaporation coefficient, W_{H_2O} is the molar mass of water, R is the universal gas constant, T_g is the gas phase temperature, σ represents surface tension, d_b is the bubble diameter, P_{sat} is the saturation pressure corresponding to the temperature at gas-liquid interphase, ϕ_g is the volume fraction of gas mixture.

The heat flux due to water evaporation has a similar form as that by oxygen transfer, which is:

$$S_{H_2O,evap} = M_{H_2O,evap}\Delta H_{evap,T_l}/W_{H_2O} \quad (7)$$

$\Delta H_{evap,T_l}$ is the heat enthalpy change by per molar water evaporated at the temperature of the liquid phase, its correlation with that at the temperature of 373 K is given by Rubisov and Papangelakis (1995):

$$\Delta H_{evap,T_l} = \Delta H_{evap,373}\left(\frac{647.3 - T_l}{274.2}\right)^{0.38} \quad (8)$$

where $\Delta H_{evap,373}$ equals to 40.62 kJ/mol.

Chemical reaction of pyrite oxidation

The chemical reaction formula of pyrite oxidation is given as (Mardsen and House, 1992):

$$2FeS_2(s) + 7O_2(aq) + 2H_2O \rightarrow 2Fe^+(aq) + 4HSO_4^-(aq) \quad (9)$$

The reaction rate of pyrite oxidation is expressed by a first order reaction, that is:

$$R_{reac} = kC_{O_2,bl}\phi_l \quad (10)$$

here k is the reaction rate coefficient of pyrite oxidation, it is given as

$$k = A\exp\left(-\frac{E_a}{RT_l}\right) \quad (11)$$

where A is called the pre-exponential factor or the frequency factor, 4.6833×10^5 s^{-1}. E_a is called the activation energy of pyrite oxidation reaction, 65.8 kJ/mol (Rajko and Katarina, 2000). Through Equ. (9) and (10), it is easy to evaluate the consumption rate of aqueous oxygen in the unit of $kg/(m^3 \cdot s)$ by the following expression:

$$M_{O_2,conp} = 7R_{reac}W_{O_2} \quad (12)$$

Pyrite oxidation is a highly exothermic reaction and the heat flux by pyrite oxidation reaction is

$$S_{reac} = R_{reac}\Delta H_{reac} \quad (13)$$

where ΔH_{reac} is the reaction enthalpy change of pyrite oxidation, -4037 kJ/mol.

CFD governing equations for pyrite oxidation

For any CFD problem, there are three conservation laws, namely mass conservation, momentum conservation and energy conservation. As to multi-phase multi-component flow, the three conservation laws are suitable for each phase and each component. However all components in a phase are mixed at molecular level and each component shares the same velocity, temperature and pressure with the phase. Therefore only mass conservation is considered for each component in a multi-phase multi-component

Mass Conservation	$\frac{\partial}{\partial t}\left(\phi_g \rho_g\right)+\nabla\cdot\left(\phi_g \rho_g u_g\right)=-M_{O_2,tran}+M_{H_2O,evap}$	(14)
	$\frac{\partial}{\partial t}\left(\phi_l \rho_l\right)+\nabla\cdot\left(\phi_l \rho_l u_l\right)=M_{O_2,tran}-M_{H_2O,evap}$	(15)
	$\phi_g+\phi_l=1$	(16)
Momentum Conservation	$\frac{\partial}{\partial t}\left(\phi_g \rho_g u_g\right)+\nabla\cdot\left(\phi_g \rho_g u_g u_g\right)=-\phi_g\nabla P-\nabla\cdot\left(\phi_g \tau_g\right)+\phi_g \rho_g g+C_D\left(u_l-u_g\right)$	(17)
	$\frac{\partial}{\partial t}\left(\phi_l \rho_l u_l\right)+\nabla\cdot\left(\phi_l \rho_l u_l u_l\right)=-\phi_l\nabla P-\nabla\cdot\left(\phi_l \tau_l\right)+\phi_l \rho_l g+C_D\left(u_g-u_l\right)$	(18)
Energy Conservation	$\frac{\partial}{\partial t}\left(\phi_g \rho_g h_g\right)+\nabla\cdot\left(\phi_g \rho_g u_g h_g\right)=-\nabla\cdot\left(\phi_g q_g\right)+\phi_g \rho_g g\cdot u_g+C_h\left(T_l-T_g\right)+S_{O_2,tran}+S_{H_2O,evap}$	(19)
	$\frac{\partial}{\partial t}\left(\phi_l \rho_l h_l\right)+\nabla\cdot\left(\phi_l \rho_l u_l h_l\right)=-\nabla\cdot\left(\phi_l q_l\right)+\phi_l \rho_l g\cdot u_l+C_h\left(T_g-T_l\right)-S_{O_2,tran}-S_{H_2O,evap}-S_{reac}$	(20)
Component Conservation	$\frac{\partial}{\partial t}\left(\phi_g \rho_g Y_{H_2O,g}\right)+\nabla\cdot\left(\phi_g \rho_g u_g Y_{H_2O,g}\right)=\nabla\cdot\left(\phi_g D_{H_2O,g}\nabla Y_{H_2O,g}\right)+M_{H_2O,evap}$	(21)
	$Y_{H_2O,g}+Y_{O_2,g}=1$	(22)
	$\frac{\partial}{\partial t}\left(\phi_l \rho_l Y_{O_2,l}\right)+\nabla\cdot\left(\phi_l \rho_l u_l Y_{O_2,l}\right)=\nabla\cdot\left(\phi_l D_{O_2,l}\nabla Y_{O_2,l}\right)+M_{O_2,tran}-M_{O_2,conp}$	(23)
	$Y_{O_2,l}+Y_{slurry}=1$	(24)

Table 1: CFD model of gas-liquid two-phase flow for the pyrite oxidation process.

flow. The momentum conservation and energy conservation of each component are the same with its surrounding phase. The CFD governing equations correspond to the conservation laws for pyrite oxidation system are given in Table 1. The drag coefficient between two phases was evaluated using generalized correlations of Alexander and Mosi. Other less important couplings due to lift forces and virtual mass effect were neglected. The k-ε model was used to model the turbulence. Simulations were performed in 2D using CFX 5.5.

Definitions of flow patterns for gas-liquid two-phase flow in horizontal pipes

Flow pattern represents the state that a multi-phase flow appears under a given operating condition in a certain device. For gas-liquid two-phase flow in horizontal pipes, Govier and Aziz (1972) presented a detailed description of all possible flow patterns relevant to operating conditions such as superficial gas and liquid velocities. According to the continuity of fluids, dispersed or continuous, full range of flow patterns can be classified into four groups, namely bubble flow, slug flow, wave flow and mist flow, as shown in Table 2.

Flow Patterns / Phases	Bubble flow	Slug flow	Wave flow	Mist flow
Gas phase	D	D	C	C
Liquid phase	C	D	C	D

Table 2: Classification of flow patterns based on the continuity of fluids. (C---Continuous; D---Dispersed)

Most research focus on bubble flow which can exist over a wide range of operating conditions. There is little agreement as to the definition of bubble flow. Bubble flow is divided into several sub-flow patterns by some authors, for example, dispersed bubble flow and elongated bubble flow (Andreussi et al, 1999) or dispersed bubble flow and bubble flow (Barnea, 1987).

In the present paper the dominant mechanism (Li and Kwauk, 1994) is adopted to define the full range of flow patterns for gas-liquid two-phase flow in horizontal pipes. If gas flow rate is increasing gradually with a constant liquid flow rate, or vice versa, three dominant conditions between the gas phase and the liquid phase alternatively appear. The three dominant conditions are called respectively gas dominated, gas-liquid coordinated and liquid dominated.

In the gas dominated regime, liquid exists in droplets and its movement is controlled by the gas phase, for instance, mist flow. In the liquid dominated regime, gas takes on bubbles and its movement is controlled by the liquid phase, for example, dispersed bubble flow. In gas-liquid coordinated regime, none of the gas phase and the liquid phase can dominate the other one, such as buoyant bubble flow, slug flow and wave flow.

Of all the above-mentioned flow regimes, dispersed bubble flow and buoyant bubble flow have produced more interests because of their capability for obtaining large interfacial areas for heat and mass transfer. The commonality of the two regimes is the existence of bubbles. Therefore sometimes they are called bubble flow by mistake without discrimination. In fact there is a big difference between dispersed bubble flow and buoyant bubble flow, namely the role of buoyancy. In dispersed

bubble flow the buoyancy can be neglected compared with the liquid action. In this case the bubbles move in horizontal pipes with some symmetry about the pipe axis. While in the buoyant bubble flow regime, the buoyancy plays an important role as well as the liquid action. Therefore the movement of bubbles in this regime is asymmetrical about the pipe axis. Through the effect of buoyancy, bubbles are observed to move from the pipe bottom to the pipe top. The buoyant flow regime is widely investigated by many researchers, for example, Andreussi et al, 1999; Iskandrani and Kojasoy, 2001; Beattie, 1996; Holmes and Russel, 1975, and so on.

Simulation results and discussions

As shown in Figure 2., the horizontal pipe for simulation is 2 m long and the diameter is 2 cm. There are four holes with a diameter of 2 mm for oxygen injection. Hot slurry suspension containing 20% pyrite fine particles enter the pipe inlet. Based on the datum about flow patterns from Govier and Aziz (1972), operating conditions for dispersed bubble flow and buoyant bubble flow are determined. That is, for dispersed bubble flow, the mass flow rate of oxygen is $3.17\times10^{-5} kg/s$ and the mass flow rate of slurry suspension is $0.518 kg/s$; for buoyant bubble flow, the mass flow rate of oxygen is $3.17\times10^{-4} kg/s$ while the mass flow rate of slurry suspension is the same as $0.518 kg/s$.

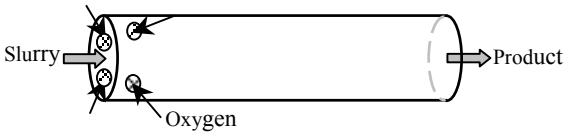

Figure 2: Pipe scheme for simulation.

Figure 3 gives the simulation result of radial void fraction distribution for pyrite oxidation and compares it with the experimental result of radial void fraction distribution for air-water system. Both systems are in buoyant bubble flow regime. Although air-water system is widely used as the object in many experiments, gas-liquid two-phase flow of pyrite oxidation in this paper is analogous to air-water system. For example, in both systems the difference in densities between the gas phase and the liquid phase has a similar value. Therefore it is reasonable to compare the tendency of simulation results for pyrite oxidation process with the experimental results reported for air-water system.

The simulation result is taken from the vertical line at the centre of the pipe axis. In Figure 3, dimensionless radial position at r/R = -1 represents the bottom of the pipe, while the position at r/R = 1 denotes the top of the pipe. It is evident that the buoyant bubble flow void fraction increases from the pipe bottom to the pipe top. This indicates that gas bubbles tend to migrate toward the pipe top and build up there due to the buoyancy action. Similar experimental results have also been reported by Iskandrani and Kojasoy (2001) and Andresussi et al. (1999).

Severe asymmetric character about the pipe axis of velocity profiles is obtained in buoyant bubble flow, as shown in Figure 4. In the bottom part of the pipe, both the gas phase and the liquid phase appear to be in fully-developed turbulent flow obeying the $1/7^{th}$ law with a sharp increase of velocity toward the pipe centre. In the central area near pipe axis, liquid moves forward with a constant velocity, whereas gas is still rising to the pipe top with an increasing velocity.

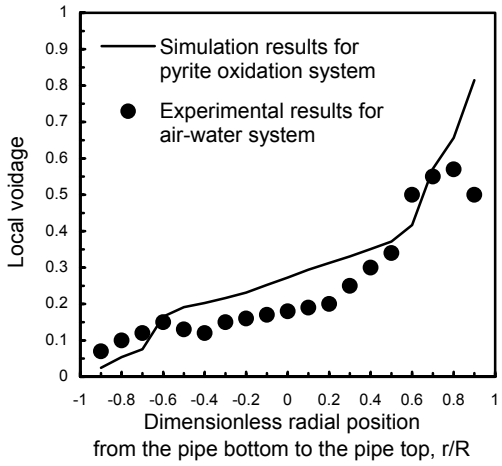

Figure 3: Comparison of radial voidage trend between simulation results for pyrite oxidation and experimental results for air-water system (Beattie, 1996) in buoyant bubble flow regime.

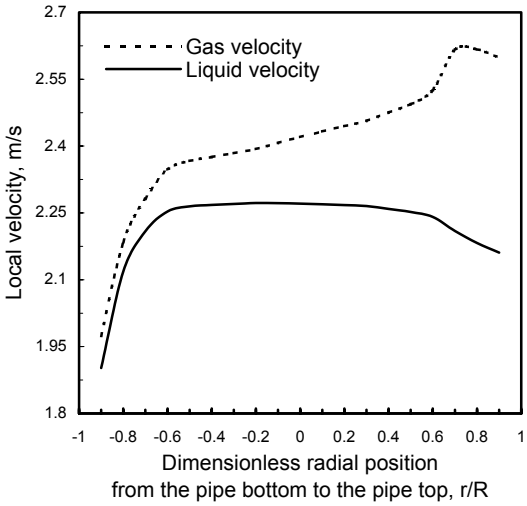

Figure 4: Radial distribution of local gas velocity magnitude and liquid velocity in buoyant bubble flow at z/L = 0.5.

In the top section of the pipe where an amount of gas is accumulating, the movement of gas with the largest velocity is less restricted by the liquid phase. Due to the action by the pipe wall, gas velocity decreases near the wall boundary. Therefore a velocity peak near the pipe wall region is exhibited by the gas velocity profile. If only a single liquid phase moves in the pipe, the liquid velocity in the pipe top region will almost be equal to the velocity in the bottom region with a small value. But because of the existence of the gas phase with large velocity in the pipe top section, the liquid phase is dragged forward at that region by the gas phase. Hence the liquid velocity in the top region is higher than the velocity in the bottom region. This is the reason for the asymmetric distribution

of liquid velocity. Another interesting phenomenon observed from Figure. 4 is that of an obvious slip velocity which appears in the pipe top region while a small slip velocity exists in the bottom part of the pipe. The slip velocity, because of the big difference in densities between phases, is an important characteristic of two-phase flow. It is evident to see that the liquid phase occupies a dominant position in the pipe bottom section where the movement of the gas phase is controlled by the liquid phase with a little slip velocity between them. Whereas, in the top part of the pipe there is a large slip velocity. The reason for this big slip velocity is that gas moves with less limitation by liquid and liquid velocity tends to decrease due to the boundary conditions.

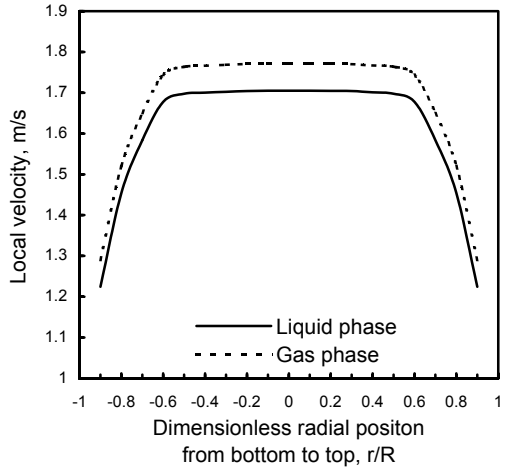

Figure 5: Radial distribution of local gas velocity and liquid velocity in dispersed bubble flow at z/L = 0.5.

The radial velocity distribution of the gas phase and the liquid phase in dispersed bubble flow (Figure 5) totally differs from that in the above buoyant bubble flow. In the dispersed bubble flow, gas bubbles move in a fairly symmetric flow. In both the top region and the bottom region, gas velocity and liquid velocity decrease sharply due to the wall effect. The slip velocity in the dispersed bubble flow is not as distinctive as in the buoyant bubble flow. As evident from Figure 3, the gas hold up near the walls was nearly unity indicating that in dispersed bubble flow, gas migrated to the pipe wall from all directions with equivalent chances, thus a gas layer is formed near the pipe wall region. However, in buoyant bubble flow gas tends to move to the top section of the pipe, thus a gas rich thick layer is formed in that region. The void fraction decreases with decreasing mass flow rate of gas at a constant flow rate of liquid. The cross-sectional distribution of void fraction in the two bubble flow patterns indicates that the degree of asymmetry decreases with increasing liquid flows or decreasing gas flow (Iskandrani and Kojasoy, 2001). From the aspect of contacting areas between reactants, the gas accumulation in the top part of the pipe will result in low chemical reaction rate compared to that by fully dispersed bubble flow. For pyrite oxidation in this paper, the oxygen consumption rate in buoyant bubble flow should be smaller than that in dispersed bubble flow. The model calculations confirm this conclusion. For example, the oxygen consumption rate in buoyant bubble flow is only 6.99%, while it can be as high as 20.7% in dispersed bubble flow. Because the oxygen mass flow rate in buoyant bubble flow is ten times that in dispersed bubble flow, the conversion rate of pyrite particles is still higher than in the dispersed bubble flow. From economical point, the flow pattern of dispersed bubble flow has advantage over buoyant bubble flow. But the disadvantage of dispersed bubble flow is its low conversion rate of pyrite particles.

The profile along the pipe length of dissolved oxygen molar concentration (Figure 6) also supports the above conclusion. In buoyant bubble flow, more oxygen moves to the pipe top region and most oxygen in that region has less contact area with liquid slurry. Therefore, less oxygen is transferred to liquid slurry in buoyant bubble flow. In dispersed bubble flow, oxygen bubbles are distributed in the liquid slurry uniformly, therefore the contact area between oxygen and liquid slurry become bigger. Thus the consumption rate of oxygen increases in the dispersed bubble flow.

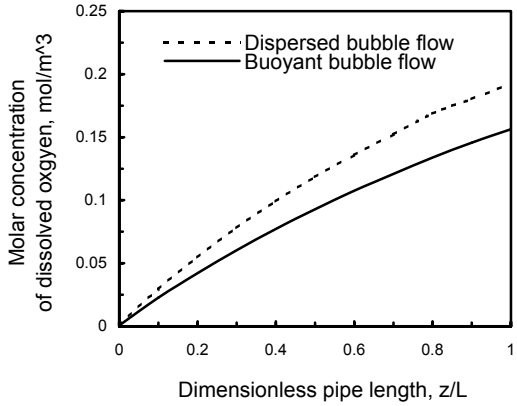

Figure 6: Comparison of molar concentration of dissolved oxygen in two bubble patterns.

Because the mass flow rate of oxygen in buoyant bubble flow is higher than that in dispersed bubble flow with both under the same mass flow rate of slurry suspension, the mass fraction of water vapour in gas mixture must be less in buoyant bubble flow than the dispersed bubble flow, as shown in Figure 7.

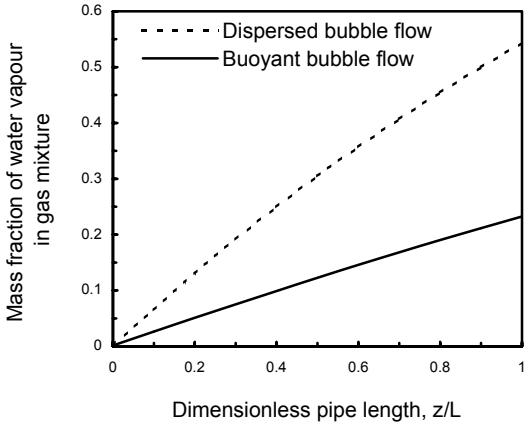

Figure 7: Comparison of mass fraction of water vapour in two bubble patterns.

CONCLUSIONS

Pyrite oxidation in horizontal pipe reactors belongs to a gas pseudo-liquid two-phase multi-component flow. A comprehensive computational fluid dynamic model has been developed based on the analysis of the physical processes and chemical reactions occurring in pyrite oxidation system. Due to the existence of the gas phase, the identification and judgement for the type of flow pattens become important before exploring the dynamics. According to the dominant mechanism, this paper present a new classification for flow patterns of gas-liquid two-phase flow in horizontal pipes, namely, gas dominated (such as dispersed bubble flow), liquid dominated (such as mist flow) and gas-liquid coordinated (for instance, buoyant bubble flow, slug flow and wave flow).

Considering the contact area between reactants, much interests focus on bubble flow including dispersed bubble flow and buoyant bubble flow. The dynamics of these two different bubble flows were investigated in a horizontal pipe with 2 m length and 2 cm of diameter by the CFD model. Four holes for oxygen injection with a 2 mm diameter each were dug on the wall of the pipe near the inlet location. For the two cases, the mass flow rate of slurry was kept at the same value of 0.518 kg/s. But the mass flow rates of oxygen for the two bubble flow patterns were different. $3.17 \times 10^{-5}\ kg/s$ for dispersed bubble flow while $3.17 \times 10^{-4}\ kg/s$ was used for buoyant bubble flow.

In buoyant bubble flow, gas tends to migrate toward the pipe top. The void fraction in this flow regime increases from the pipe bottom to the pipe top. The simulation results were consistent with experimental reports from the literature. The flow in the bottom part of the pipe exhibits a $1/7^{th}$ power law profile, whereas, in the top of the pipe a different flow exists. The gas velocity is largest in the top region and a velocity peak appears near the pipe wall. Due to the interaction by gas, the liquid velocity in the top part of the pipe differs from the velocity distribution in the bottom section of the pipe because of the wall effects.

In dispersed bubble flow, the buoyancy force can be neglected compared to the liquid action. The profiles of both void fraction and velocity show a certain symmetry about the pipe axis. Therefore this flow regime can offer larger interfacial contact areas between reactants than buoyant bubble flow. This must enhance the oxygen consumption rate. The model calculation results also confirm this conclusion, for example, the oxygen consumption rate in dispersed bubble flow can be as high as 20.7%, while this is only 6.99% for buoyant bubble flow. However the conversion rate of pyrite particles in buoyant bubble flow is still higher due to its bigger mass flow rate of oxygen input. Dispersed bubble flow can make much more oxygen dissolve than buoyant bubble flow. Therefore from an economic point, dispersed bubble flow is better than buoyant bubble flow although it has a lower conversion rate of pyrite particles.

REFERENCES

ANDREUSSI, P., PAGLIANTI, A. and SILVA, F. S., (1999), "Dispersed bubble flow in horizontal pipe", *Chemical Engineering Science,* **54**, 1101-1107.

BARNEA, D., (1987), "A unified model for predicting flow-pattern transitions fro the whole range of pipe inclinations", *International Journal of Multiphase Flow*, **13**, 1-12.

BEATTIE, D. R. H., (1996), "Flow characteristics of horizontal bubbly pipe flow", *Nuclear Engineering and Design*, **163**, 207-212.

CAREY, V. P., (1992), *Liquid-Vapor Phase-Change Phenomena: An Introduction to the Thermophysics of Vaporization and Condensation Process In Heat Transfer Equipment.* Hemisphere, Washington, DC, 112-120.

EAMES, I. W., MARR, N. J. and SABIR, H., (1997), "The evaporation coefficient of water: a review", *International Journal of Heat and Mass Transfer*, **40**, 2963-2973.

FELICE, R. D., (2000), "The pseudo-fluid model applied to three-phase fluidisation", *Chemical Engineering Science*, **55**, 3899-3906.

GOVIER, G. W. and AZIZ, K., (1972), *The flow of complex mixtures in pipes*. New York, Van Nostrand Reihold Company.

HOLMES, T. L. and RUSSEL, T. W. F., (1975), "Horizontal bubble flow", *International Journal of Multiphase Flow*, **2**, 51-66.

HUA, J.and WANG, C. H., (2000), "Numerical simulation of bubble-driven liquid flows" *Chemical Engineering Science*, **55**, 4159-4173.

ISKANDRANI, A. and KOJASOY G., (2001), "Local void fraction and velocity field description in horizontal bubbly flow", *Nuclear Engineering and Design*, **204**, 117-128.

LI, J. and KWAUK, M., (1994), *Particle-Fluid Two-Phase Flow,* Beijing, Metallurgical Industry Press.

MARDSEN, J. and HOUSE, L., (1992), *The Chemistry of Gold Extraction,* Chichster, Ellis Horwood.

RAJKO, Z. V. and KATARINA, P. C., (2000), "Manganese leaching in the FeS_2-MnO_2-O_2-H_2O system at high temperature in an autoclave", *Hydrometallurgy*, **55**, 79-92.

RUBISOV, D. H. and PAPANGELAKIS, V. G., (1995), "Model-based analysis of pressure oxidation autoclave behaviour during process upsets", *Hydrometallurgy*, **39**, 377-389.

VAN Der Welle, R., (1985), "Void fraction, bubble velocity and bubble size in 2-phase flow", *International Journal of Multiphase Flow*, **11**, 317-345.

ZHANG, J. T., WANG, B. X. and PENG, X. F., (2001), "Thermodynamic aspects of the shift of concave liquid-vapour interfacial phase equilibrium temperature and its effect on bubble formation" *International Journal of Heat and Mass Transfer*, **44**, 1681-1686.